Polymer 50 (2009) 4635–4643

Contents lists available at ScienceDirect

Polymer

journal homepage: www.elsevier.com/locate/polymer

Thermal properties of poly(ethylene succinate) nanocomposite

Suprakas Sinha Ray*, Mamookho E. Makhatha

National Centre for Nano-Structured Materials, Council for Scientific and Industrial Research (CSIR), Pretoria 0001, Republic of South Africa

ARTICLE INFO

Article history:
Received 7 June 2009
Received in revised form
7 July 2009
Accepted 16 July 2009
Available online 19 July 2009

Keywords:
Poly(ethylene succinate)
Nanocomposites
Thermal properties

ABSTRACT

This article describes the thermal properties of clay-containing poly(ethylene succinate) (PES) nanocomposite. The nanocomposite of PES with organically modified montmorillonite (o-mmt) has been prepared by solution-intercalation-film-casting technique. Small-angle X-ray scattering patterns and transmission electron microscopy observations show the homogeneous dispersion of silicate layers in the PES matrix. The crystallization and melting behaviors of the PES matrix in the presence of dispersed silicate layers have been studied by differential scanning calorimeter, polarized optical microscope, and wide-angle X-ray scattering. Results show that the incorporation of o-mmt stops the super-cooling effect and accelerates the mechanism of nucleation and crystal growth of PES matrix significantly. The incorporation of o-mmt also improves the thermal stability of neat PES dramatically.

1. Introduction

In recent years, thermoplastic biodegradable polyesters, whether synthesized from chemical feed-stocks or from agriculture products, have received a great deal of research attention due to their potential applications in the field of environmental benign plastic products [1–4]. PES, a condensate of succinic acid and ethylene glycol, is such an interesting thermoplastic polyester with properties comparable to many commodity plastics such as polypropylene, polyethylene, etc. [5]. Biodegradation is undoubtedly one of the most important properties of PES and a number of articles have recently been published on the nature of PES degradation [6–9]. For example, Transengco and Tokiwa [6] investigated the distribution and population of PES-degrading microorganisms at a temperature of 50 °C using the plate count and clear zone methods. They also studied the biodegradation effect of a PES-utilizing isolate on other polyesters such as polylactide (PLA), poly(butylene succinate), etc. The results showed that the presence of PES-degrading microorganisms is fairly limited compared to the other polyesters. In another work, Tezuka et al. [7] reported the degradation pattern of PES in natural environments by isolating the mesophilic PES-degrading strains. On the basis of their experimental results, they concluded that the mesophile is an important PES degrader in natural environments. Further, Ishii et al. [8] isolated and identified a group of PES-degrading filamentous fungi, and investigated the process of PES degradation by the filamentous fungal isolate strain NKCM1003.

Unlike microbial polyesters, such as poly(3-hydroxy butyrate) (PHB) that is susceptible to degradation in various environments, the degradation of PES was found to be strongly dependent on environmental factors [10,11]. For example, Kasuya et al. [10] reported the influence of different natural waters on the biodegradability of eight different types of polyesters including PES. To study the rate of degradation, they used both bio-chemical oxygen demand and weight loss of samples at 25 °C. Results have shown that the rate of degradation of polyesters not only depends on the chemical structure of monomeric units, but also on the source of natural water. However, in many applications, increasing the crystallization speed of PES is desired since in its amorphous form, the range of application of PES is severely limited because only the crystalline PES phase can confer useful mechanical and other physical properties. Furthermore, the degradability of biodegradable polymers is also influenced strongly by the degree of crystallinity. For example, Li and McCarthy investigated the enzymatic degradation characteristics of two representative PLA polymers, such as poly(l-lactide) (PLA_{100}) and poly(DL-lactide) (PLA_{50}) [12]. They used proteinase K as an enzyme to study the degradation behavior of PLA. The results showed that proteinase K is able to strongly accelerate the degradation of PLA polymers and up to a certain degree of crystallinity (~26%); PLA_{100} and PLA_{50} exhibited the same degree of degradability. However, above the crystallinity value, the degradation rate of PLA_{100} decreases with an increase in crystallinity.

Recently, a number of articles have appeared on the crystallization behavior and morphology of PES in the presence of other polymers and nucleating agents [13–18]. For example, Al-Salah [16] studied the melting and crystallization characteristic of PES in the

* Corresponding author. Tel.: +27 12 841 2388; fax: +27 12 841 2229.
E-mail address: rsuprakas@csir.co.za (S. Sinha Ray).

0032-3861/$ – see front matter © 2009 Elsevier Ltd. All rights reserved.
doi:10.1016/j.polymer.2009.07.025

presence of PBH. Blends of PES and PBH were prepared by melt-mixing. During isothermal crystallization, the presence of the PHB component showed a wide variety of morphologies. On the other hand, blends of PES with polycarbonate showed a single glass transition temperature. The miscibility and crystallization behaviors of PES with PLA were studied by Chen et al. [17]. According to them, the crystallization mechanisms of PES did not change in the presence of PLA; however, the isothermal crystallization rate of PES was found to decrease with an increase in PLA content in blends. A similar observation was also reported by Qiu et al. in the case of PES/poly(ethylene oxide) blends [18].

However, up to this date no attention has been given to using nano-dimensional clay particles as a means of increasing the crystallinity and improving the thermal and mechanical properties of PES. Clay particles have a huge surface area [mmt has the specific surface area (S_O) of about 700–800 m^2/g] and are able to be well dispersed in the polymer matrix [19,20]. Therefore, clay particles can act as a strong nucleating agent for PES crystallization.

The present study focuses on the study of non-isothermal crystallization and melting behaviors of the PES matrix in the presence of very high-aspect silicate particles, by using differential scanning calorimeter (DS), polarized optical microscope, and small- and wide-angle X-ray scattering. Finally, the thermal stability of pure PES and nanocomposite was studied using a thermogravimetric analyzer. Before all of this, however, there is a brief discussion on the structure and morphology of PES/o-mmt nanocomposite.

2. Experimental part

2.1. Materials

PES used in this study is a commercial product from Aldrich Chemical, which according to the supplier, has a weight-average molecular weight, $M_w = 181$ kg/mol. PES was dried under vacuum at 50 °C for 36 h prior to use. o-mmt used in this study was Cloisite®30B (C30B), purchased from the Southern Clay Products. According to the supplier, the original clay is mmt and modified with 30 wt% of methyl tallow bis(2-hydroxylethyl) quaternary ammonium salt. The chemical structures of PES and methyl tallow bis(2-hydroxylethyl) quaternary ammonium are presented in parts (a) and (b) of Fig. 1, respectively.

The reason for choosing C30B as an organoclay in this study is due to the closest value of organic modifier solubility parameter with that of PES. The solubility parameters (δ) for PES and the organic modifier, methyl tallow bis(2-hydroxyethyl) quaternary ammonium, were roughly calculated from the group contribution methods of Fedors [21]. The values of δ for PES and 30B are 19.9 and 21.5 $J^{1/2}\,cm^{-3/2}$, respectively.

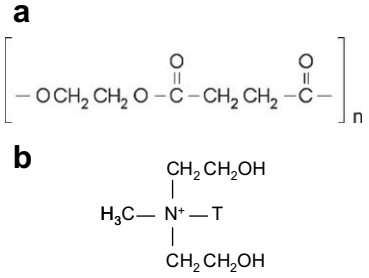

Fig. 1. (a) Molecular structure of poly(ethylene succinate) and (b) Chemical structure of bis(2-hydroxylethyl) quaternary ammonium used to modify pristine montmorillonite. 'T' represents tallow (~65% C18; ~30% C16; ~5% C14).

2.2. Nanocomposite preparation

PES nanocomposite containing 5 wt% C30B was prepared using the solution-intercalation-film-casting technique. 5 g of PES was dissolved in 20 ml of chloroform ($CHCl_3$) at room temperature (24 °C). C30B dispersion in $CHCl_3$ was obtained by suspension of well-dried C30B in another conical flask. Both PES solution and C30B suspension were sonicated separately for 30 min and subsequently mixed. The final mixture was further sonicated for 30 min at room temperature. The mixture was then cast on a glass surface and dried in a vacuum oven for 12 h. The solvent-cast nanocomposite film was compression molded into a sheet of ~0.6 mm thickness, using a Carver Laboratory press at 135 °C for 10 min. These compression-molded sheets were then used for various characterizations. For comparison purposes, a PES sheet without o-mmt was prepared using the same processing technique.

2.3. Characterization

2.3.1. Small- and wide-angle X-ray scattering (SWAXS) study

To check the degree of dispersion of silicate layers in the PES matrix, SWAXS experiments of pure C30B powder and annealed (at 50 °C for 5 h) compression-molded sheets of pure PES and nanocomposite were performed with the SAXSess system from Anton Paar GmbH, operated at 40 kV and 50 mA. The radiation used was a Ni filtered CuKα radiation source with a wavelength of 0.154 nm (PAN analytical). The two-dimensional (2-D) detector was a curved imaging plate covering the scattering vector (q) range of 0.13–28 nm^{-1}. The read-out angles are calculated from the pixel size and the exactly known sample-to-detector distance of 264.5 mm. The obtained q scale was cross-checked by measuring silver behenate whose equidistant peak positions are known.

To find out the effect of crystal growth during non-isothermal crystallization, both pure PES and nanocomposite (annealed and compression molded) samples were heated in a paste-cell from 30 °C to 150 °C at a heating rate of 10 °C/min and then cooled down to 40 °C at a cooling rate of 10 °C/min using a TCU50 (Anton Paar GmbH) temperature control unit, attached to the SAXSess instrument. SAXS data were collected at different temperatures during both heating and cooling. The samples were kept at each temperature for 5 min including 1 min exposure time under X-ray.

2.3.2. Transmission electron microscopy (TEM)

The degree of dispersion of silicate layers in the PES matrix was investigated by means of TEM (JEOL JEM 2100), operated at an accelerating voltage of 200 kV. A nanocomposite sample was cut using cryo-ultramicrotome (−140 °C) and collected with a 300-mesh carbon coated copper grids and was observed without further treatment.

2.3.3. Differential scanning calorimeter (DSC)

The melting and crystallization behavior of compression-molded pure PES and nanocomposite samples were conducted with the DSC (TA-Instruments model Q2000 series), under a constant nitrogen flow of 50 ml/min. The samples' weights were maintained at low levels (6–9 mg) for all measurements in order to minimize any possible thermal lag during the scans. The instrument was calibrated by employing the temperature and heat of fusion of indium standard, and the base line was checked according to the TA-Instruments protocols. To study the non-isothermal crystallization behavior, samples were first melted at 120 °C at a heating rate of 20 °C/min, kept at that temperature for 5 min to destroy any previous thermal history, and cooled to −60 °C at constant cooling rates of 2, 5, 10, 15, and 20 °C/min. To study the effect of the crystallization rate on the melting behavior, samples were heated from −60 °C to 120 °C at

a heating rate of 20 °C/min as soon as cooling was finished. Each reported result is an average of three different measurements.

To separate the heat capacity and kinetic related components during heating of pure PES and the nanocomposite samples, temperature-modulated DSC (TMDSC) experiments were carried out using the same DSC instrument with a constant nitrogen flow of 50 ml/min. TMDSC generally applies a sinusoidal temperature oscillation (modulation) on a conventional heating DSC and allows the total heat flow (as obtained from conventional DSC) to be separated into the heat capacity related (reversible) and kinetic (non-reversible) components. The heat capacity was calibrated with a sapphire sample. The heating rate was 2 °C, with an amplitude of ±0.796 °C, and a period of 60 s. The TMDSC was started as soon as cooling from melt was finished.

2.3.4. Spherulite morphology

The spherulite structure of both pure PES and nanocomposite samples during non-isothermal crystallization was studied with a Carl-Zeiss Imager Z1M polarized optical microscope (POM) equipped with a Linkam hot stage (Linkam Scientific Instruments Ltd, UK). Compression-molded thin films were placed in between two covering glasses and placed on a Linkam hot stage, mounted on an optical microscope. Samples were melted at 120 °C at a heating rate of 20 °C/min, held at that temperature for 5 min and then cooled down to 40 °C at a precisely controlled cooling rate of 10 °C/min.

2.3.5. Thermogravimetric analysis (TGA)

The thermogravimetric analyses were conducted on a TGA (TA Q500 instrument) at a heating rate of 10 °C/min under pyrolytic condition, from room temperature to 800 °C. Typically three consecutive runs were conducted for each sample and averages are reported with an uncertainty of ± 1.67 °C.

3. Results and discussion

3.1. Nanocomposite structure

The structure and morphology of clay-containing polymer nanocomposites were generally probed by X-ray scattering patterns and TEM observations. X-ray scattering offers a convenient method to determine the interlayer spacing of the silicate layers in the original clay and in the intercalated polymer/clay nanocomposites, while TEM allows a qualitative understanding of the internal structure through direct visualization. The SAXS patterns of pure C30B powder and normalized background (PES was taken as background) subtracted SAXS pattern of nanocomposite are shown in Fig. 2. The mean interlayer spacing of the (001) plane ($d_{(001)}$) for the C30B powder obtained by SAXS measurement is 1.85 nm (q = 3.4 nm^{-1}, as determined by using equation $d_{spacing} = 2\pi/q$ nm). In the SAXS pattern of nanocomposite, a small peak appears at $q = 0.68$ nm^{-1}, which corresponds to the *d*-spacing of 9.2 nm. This is due to the crystalline structure of PES chains in the very small-angle region (see inset of Fig. 2). However, it is very interesting to note that this crystalline arrangement of the PES matrix remains almost unaltered after nanocomposite formation with C30B.

On the other hand, the intensity of the characteristic peak [(001) plane] of C30B is significantly reduced, and a broad peak is observed at $q = 1.7$ nm^{-1} [$d_{(001)} = 3.7$ nm]. Such an observation indicates that most of the silicate layers lost their initial stacking and are highly dispersed in the PES matrix. This may be due to the favorable interfacial interactions between the 'CO' groups on the PES backbone with the hydroxyl groups on C30B surfaces. Furthermore, in the SAXS pattern of nanocomposite another broad peak at $q = 3.5$ nm^{-1} is observed. After calculation, it is confirmed that this peak is from the (002) plane of the silicate layers dispersed in the PES matrix [22].

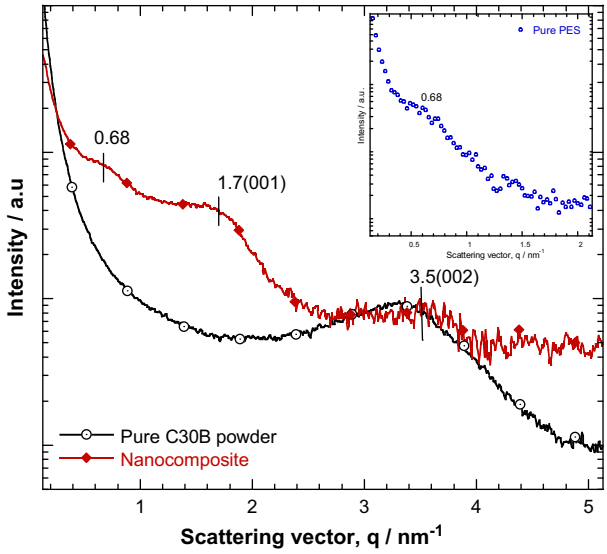

Fig. 2. The normalized small-angle X-ray scattering (SAXS) pattern of pure C30B powder and normalized background (polymer was considered as background) subtracted SAXS pattern of nanocomposite. The small peak at $q = 0.68$ nm^{-1} is due to the crystalline structure of polymer (see inset SAXS pattern of pure polymer).

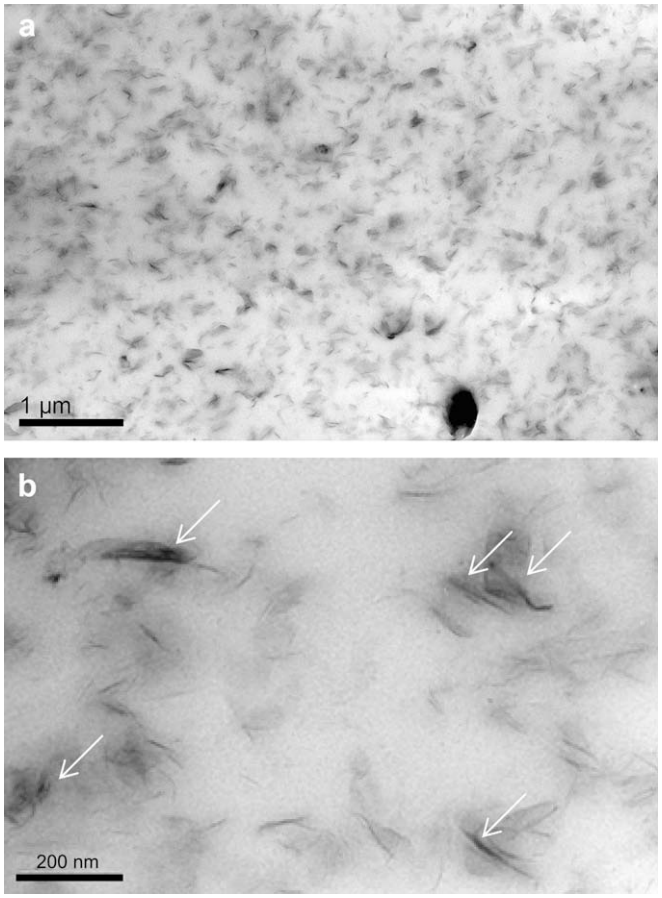

Fig. 3. Bright field transmission electron microscopy images of nanocomposite containing 5 wt% C30B at two different magnifications, where black entities are the dispersed silicate layers. Results show the formation of disorder intercalated nanocomposite where both single and stacked (marked by arrow in Fig. 3b) silicate layers coexisting.

To support the observed SAXS pattern of nanocomposite, the degree of dispersion of silicate layers in the PES matrix was studied by TEM. Fig. 3a and 3b shows the TEM bright field images of PES nanocomposite containing 5 wt% C30B. The figures show both larger views, illustrating the dispersion of the silicate layers in the PES matrix, and a higher magnification, permitting the observation of discrete silicate layers. TEM images for nanocomposite reveal that there are some intercalated and disordered and/or exfoliated silicate layers coexisting in the nanocomposite. This is more discernible with high magnification TEM image (marked by the arrow in the TEM images) as presented in Fig. 3b. The stacked intercalated silicate layers are responsible for a very weak and broad scattering peak as observed in the SAXS pattern (see Fig. 2) for nanocomposite, whereas the disordered and exfoliated silicate layers have no periodic stacking and thus remain X-ray silent. This kind of mixed intercalated and/or exfoliated structure originates from the chemical and size inhomogeneities of the silicate layers. Typically the larger-in lateral size-silicate layers create stacked intercalated structures, whereas the smaller layers tend to exfoliate [23,24].

The form factors obtained from SAXS analyses and TEM observations, i.e., average length (L_{clay}) and thickness (d_{clay}) of the dispersed silicate layers and the correlation length (ξ_{clay}) between them, are summarized in Table 1. It is clear from table that data calculated from SAXS patterns of nanocomposite are nicely matched with the TEM observations. Therefore, on the basis of SAXS results and TEM observation, one can conclude that the disorder intercalated structure is formed in the case of PES/C30B nanocomposite.

3.2. Crystallization behavior and morphology

To understand the effect of C30B incorporation on the crystallization behavior of the PES matrix, DSC experiments of pure PES and nanocomposite samples were carried out according to the method described in Experimental section. The crystallization exotherms of neat PES and its nanocomposite during non-isothermal crystallization from their melts at five different cooling rates are shown in Fig. 4. In the case of pure PES, when the sample was cooled at a cooling rate of 2 °C/min from melt, a small and broad peak appears at 47.5 °C. With increase in cooling rate to 5 °C/min, this peak moves to the lower temperature region. Further increase in cooling rate, a very broad peak with continuous change of crystallization enthalpy is observed. This indicates when the cooling rate from melt was more than 5 °C/min; it is very difficult for the PES matrix to crystallize and the sample stays in a supercooled state. On the other hand, for the nanocomposite sample, a sharp crystallization peak at 60 °C is observed when the sample was cooled at 2 °C/min from melt. As the cooling rate increases, this exothermic curve becomes wider and is shifted to the lower temperature region. This observation is very natural because at a higher cooling rate, the sample passes through the crystallization process so quickly that there is not enough time for the melted sample to crystallize fully. Another interesting observation is that when the nanocomposite sample cooled at a cooling rate of 15 °C/min from melt, a small shoulder peak appears at −9.6 °C. This shoulder peak moves to 14.2 °C when the sample cooled at 20 °C/min. This may be due to the growth of two different types of crystals at a higher cooling rate. On the basis of the above observations, one can conclude that the nucleating role of the delaminated silicate layers is very active and because of this active nucleation effect, PES crystals grow faster in the presence of highly dispersed silicate layers at higher cooling rates.

During non-isothermal crystallization, the true link of the obtained exotherms from DSC measurements and the nucleation behavior of the clay particles can further be examined by POM. To do POM experiments, a cooling rate of 10 °C from the melt was chosen as a model cooling rate because during injection molding the cooling rate is very fast and we are interested to see the effect of incorporation of C30B particles on the crystal growth behavior at

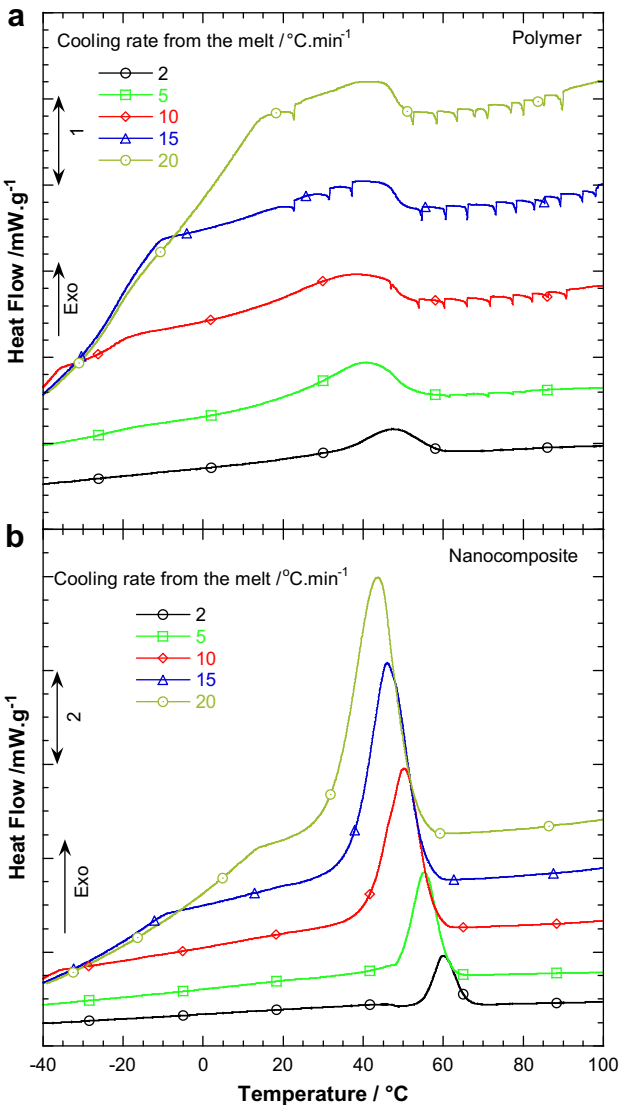

Fig. 4. The crystallization exotherms of (a) neat polymer and (b) the nanocomposite for non-isothermal crystallization from their melts (at 120 °C) at five different cooling rates ranging from 2 to 20 °C/min. Results show that it is very difficult for pure polymer sample to crystallize when cooling rate was more than 5 °C/min. However, in the case of nanocomposite sample, the dispersed silicate layers stop the super-cooling effect and accelerate the mechanism of crystal growth of polymer matrix.

Table 1
Comparison of form factors of nanocomposite obtained from SAXS pattern and TEM observation.

	SAXS	TEM[a]
Average length of dispersed clay particles, L_{clay}/nm	–	171 ± 29
Average thickness of dispersed clay particles, d_{clay}/nm	7.12[b]	6.9 ± 1.5
Aspect ratio, L_{clay}/d_{clay}	–	~24.9
Average correlation length between dispersed clay particles, ξ_{clay}		150 ± 98
The mean interlayer spacing of (001) plane, $d_{(001)}$/nm	3.7[c]	–

[a] Calculated on the basis of 6 TEM images.
[b] Calculated using Scherrer equation, $D = k\lambda/\beta\ Cos\theta$, where where k is a constant (the value generally = 0.9), λ is the X-ray wavelength ($\lambda = 0.154$ nm), β is the width of the SAXS peak (in radian unit) and is measured by the full width at half-maximum, and θ is the SAXS peak position.
[c] Calculated from (001) peak of clay particles in the SAXS pattern.

a higher cooling rate. The POM images of pure PES and nanocomposite samples taken at three different temperatures during non-isothermal crystallization from their melts at a cooling rate of 10 °C/min are presented in Fig. 5. It is clear from the images that it is very difficult for pure PES crystals to grow at a cooling rate of 10 °C/min, while PES spherulites are grown faster in the presence of highly dispersed silicate particles. This observation again supports that the nucleating role of the delaminated silicate layers is very active and because of this fast nucleation phenomenon, the PES matrix achieved a higher degree of spherulites formation at a higher cooling rate as compared to that of a pure PES matrix.

3.3. Effect of non-isothermal crystallization on melting behavior

To study the influence of non-isothermal crystallization on the melting behavior, both PES and the nanocomposite samples were heated at a heating rate of 20 °C/min directly from −60 °C as soon as the cooling was finished. Fig. 6 represents the melting behavior of pure PES and nanocomposite samples after non-isothermal crystallization; and the results are summarized in Table 2. It is clear from the figure that both samples at a slow cooling rate of 2 °C/min show three melting peaks of PES, labeled I, II, and III from low to high temperature, and two re-crystallization peaks in between them. However, with an increase in cooling rate to 5 °C/min, in the case of pure PES, I-melting disappears and a broad cold crystallization peak appears at 35.5 °C. With further increase in cooling rate, the cold crystallization phenomenon becomes more important. Such an observation is obvious because with an increase in cooling rate, it is difficult for PES polymer chains to crystallize during cooling and for this reason; more and more PES chains are crystallizing during heating. Furthermore, II-melting peak temperature systematically moves to the lower temperature region, while III-melting peak does not have any effect on cooling rates. This suggests that the crystals associated with the III-melting are more perfect than crystals associated with II-melting. Another interesting observation is that both re-crystallization peaks move towards the low temperature region with an increase in cooling rate during nano-isothermal crystallization. Again, the intensity of re-crystallization peak appears in between II- and III-melting is becoming less important with an increase in cooling rate during non-isothermal crystallization. This is also true for nanocomposites. Finally, a small relaxation peak appears at around −17.5 °C in the DSC scan of pure PES sample.

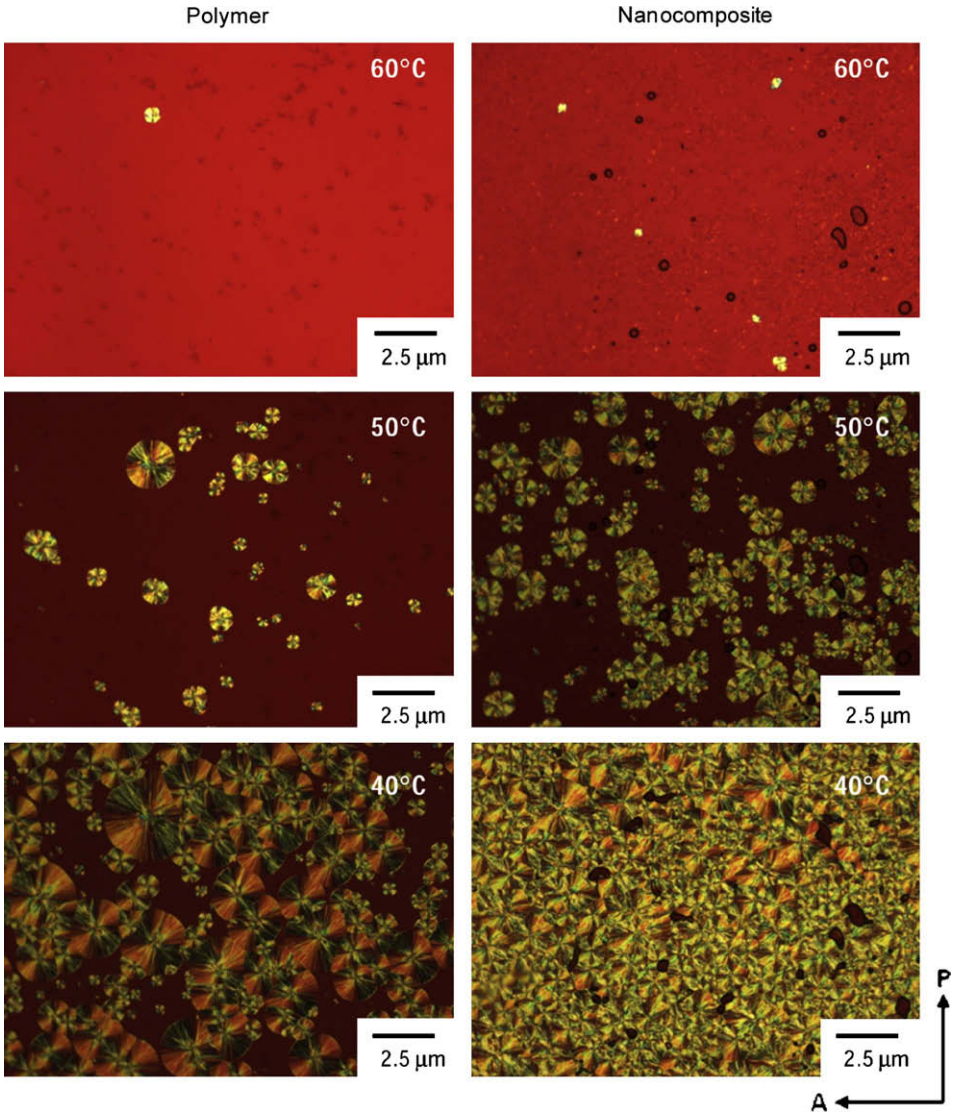

Fig. 5. The polarized optical microscopy (POM) images of pure polymer and its nanocomposite containing 5 wt% C30B at three different temperatures of 60, 50 and 40 °C during non-isothermal crystallization from their melts (120 °C) at a cooling rate of 10 °C/min. POM results support DSC thermograms.

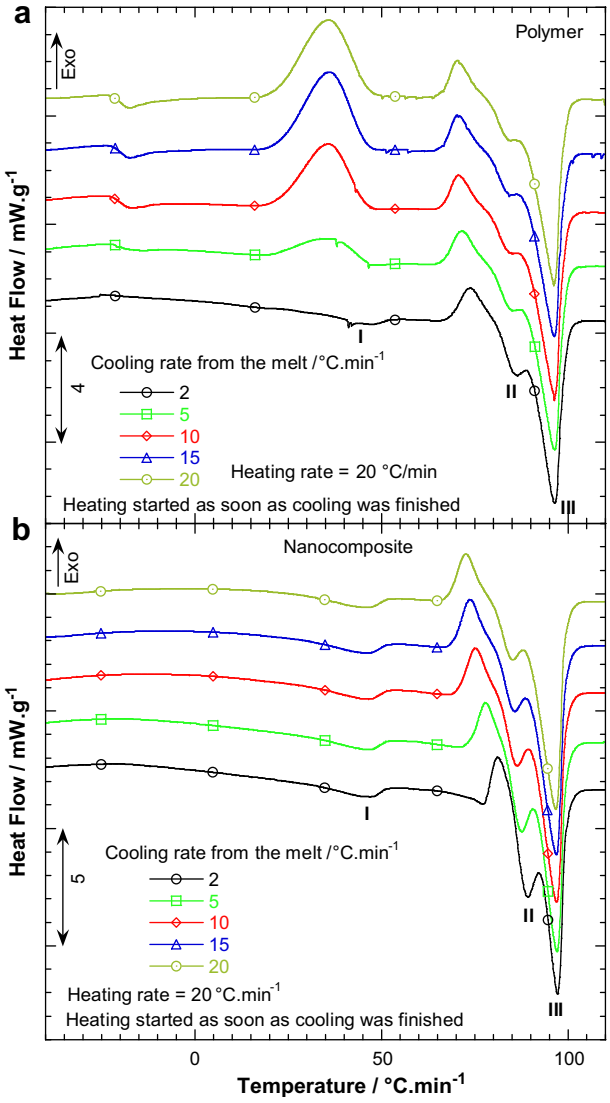

Fig. 6. Melting behaviors of (a) pure polymer and (b) nanocomposite samples after non-isothermal crystallization at five different cooling rates of 2, 5, 10, 15, and 20 °C/min from their melts (120 °C). The samples were heated at rate of 20 °C/min as soon as cooling was finished. Results show cooling rate has strong effect on the melting behavior poly(ethylene succinate) matrix.

This is due to the disentanglement of PES chains just before cold crystallization. With an increase in cooling rate, the cold crystallization phenomenon becomes more important and for this reason, this relaxation becoming more prominent with an increase in cooling rate.

On the other hand, in the case of nanocomposite, cold crystallization phenomenon does not appear. This indicates that crystallization has been completed during non-isothermal crystallization at all cooling rates. Like the pure PES, in the case of nanocomposite, II-melting peak temperature systematically moves to the lower temperature region with an increase in cooling rate; however, the positions of I- and III-melting peaks remain unaffected by the cooling rate during non-isothermal crystallization for nanocomposite sample. This suggests that the crystals associated with the I- and III-melting's are more perfect than crystals associated with II-melting. It is interesting to note that in the case of nanocomposite, all melting peaks appear at higher temperature regions than pure PES. This is due to the higher crystallinity of the PES matrix in the presence of dispersed silicate layers (see Table 2) [25].

Table 2
Rough estimation of degree of crystallinity of PES from II- and III-melting endotherms.

Sample	Cooling rate	Heat of fusion/J g^{-1} [a]	Crystallinity/% [b]
Polymer	2	34.08	18.9
	5	35.21	19.6
	10	34.99	19.4
	15	35.54	19.7
	20	35.33	19.6
Nanocomposite	2	44.85	26.9
	5	47.40	26.3
	10	49.08	27.2
	15	48.77	27.1
	20	49.33	27.4

[a] The total heat of fusion of two melting peaks (II & III) of PES evaluated by integration of the area under the edothermic peaks from heating scans after non-isothermal crystallization).
[b] Calculated using the 100% crystallinity value of PES, 180 J/g [25].

The multiple melting behaviors have already been reported for various types of semicrystalline polymers such as poly(ethylene terephthalate) [26], poly(butylene terephthalate) [27], polypropylene [28], poly(butylene succinate) [29], poly[(butylene succinate)-co-adipate] [30,31], etc. There are several models to explain the multiple melting behaviors of semicrystalline polymers, of which the two most important ones are [32,33]: (a) the presence of melting, re-crystallization, and re-melting phenomena and (b) the crystal structure modification during the heating scan. According to the first model, the first step is the melting and re-crystallization of the low melting crystallites with lower thermal stability and then the melting of the crystallites with higher thermal stability formed through the re-crystallization of the melting of the crystallites of the lower melting endotherms.

To verify the presence of the melting, re-crystallization, and re-melting phenomena of PES, TMDSC has been applied. TMDSC generally applies a sinusoidal temperature oscillation (modulation) on a heating conventional DSC and makes the total heat flow (as obtained from conventional DSC) to be separated into the heat capacity related (reversible) and kinetic (non-reversible) components. Therefore, TMDSC allows us to see that some re-crystallization process occurs as soon as PES begins to melt. Figs. 7a and 7b, respectively. Show the TMDSC traces of neat PES and nanocomposite samples that are heated at a heating rate of 2 °C/min from −60 °C as soon as cooling was finished (cooling rate from their melts was 2 °C/min). For both samples total heat flow (middle curve) is separated into the well-defined, non-reversible heat flow (top curve) and the reversible heat flow (bottom curve) (see Fig. 7).

In the case of a pure PES sample the following behaviors are observed: first, a well distinguished melting endotherm appears at 74.2 °C in the reversible cycle. Second, the intensities of two re-crystallization peaks in the non-reversible scan are higher than observed in the reversible and the total heat flow curves. Third, the melting behaviors are also observed in the non-reversible heat flow curve along with the total and reversible heat flow curves. All these observations indicate that the multiple melting behaviors of PES originate from the melting and re-crystallization of the low melting crystallites with lower thermal stability. The higher melting endotherm corresponds to the melting of the crystallites with higher thermal stability formed through the re-crystallization of the melting of the crystallites of the lower melting.

The nanocomposite sample shows almost the same behaviors as observed in the case of pure PES, but all melting and re-crystallization peaks move to the higher temperature regions. This is due to the very strong nucleation effect of dispersed silicate layers in the PES matrix [34–36].

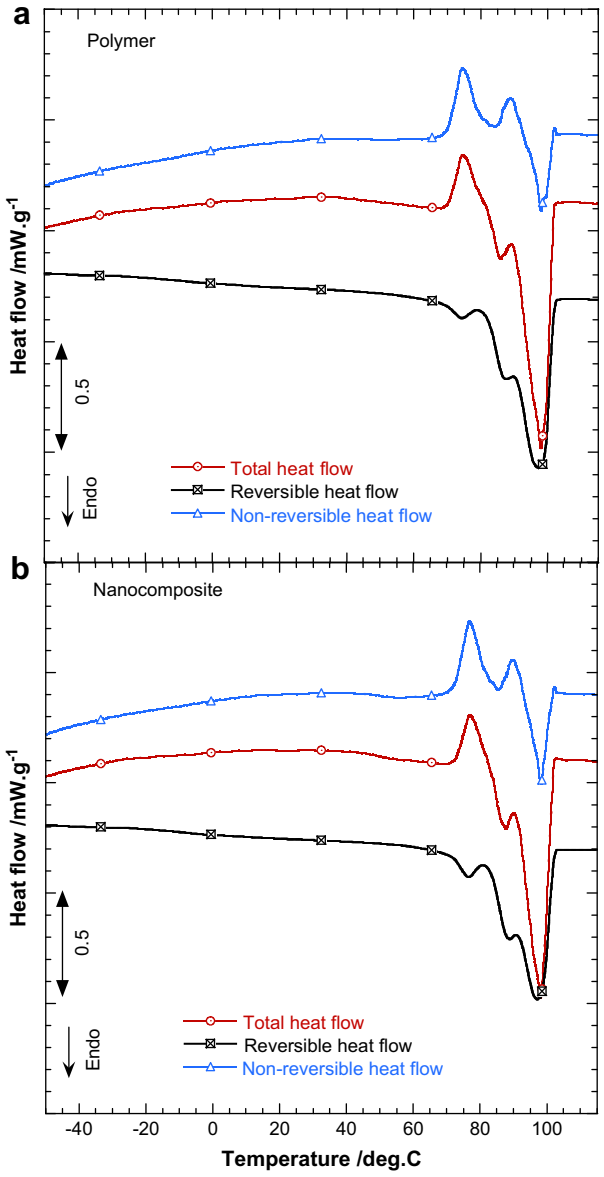

Fig. 7. Modulated differential scanning calorimeter (MDSC) thermograms of (a) pure polymer and (b) nanocomposite samples during second heating. Samples were first equilibrated at −60 °C for 20 min and then heated to 120 °C at a rate of 20 °C/min, kept at that temperature for 5 min to destroy any previous thermal history, and cooled to −60 °C at a rate of 2 °C/min. As soon as cooling was finished MDSC was started. The heating rate was 2 °C/min, with an amplitude of ±0.796 °C, and a period of 60 s.

3.4. Wide-angle X-ray scattering (WAXS) study

To find out the crystal structure modification of the PES matrix during heating, which may be responsible for the multiple melting behaviors, WAXS experiments of pure PES and nanocomposite samples were carried out at above and below the temperature of each endotherm during both heating and cooling. The samples were kept at each temperature for 5 min including a 1 min exposure time under X-ray. Fig. 8a and b, respectively, represents the one-dimensional WAXS patterns of pure PES and nanocomposite samples. It is clear from the figures that for both pure PES and nanocomposite samples, crystals are becoming more perfect with an increase in temperature; however, there is no indication of formation of new crystals or modification of any crystals. This observation again supports that the presence of melting, re-crystallization, and re-melting phenomena are responsible for the triple-melting behavior of the PES matrix.

On the other hand, the most interesting behavior is observed when both samples were cooled from their melts. Results show that it is very difficult for the pure PES sample to crystallize during cooling from its melt at a cooling rate of 10 °C/min – the sample stayed fully in its super-cooled state. However, because of the active nucleation effect of dispersed silicate layers, perfect crystals are formed during cooling from its melt at the same cooling rate. Therefore, WAXS results support the conclusions made on the basis of DSC scans and POM observations.

3.5. Thermogravimetric analyses

In this section the thermal stabilities of pure PES and nanocomposite containing 5 wt% of C30B in inert environment are discussed. The TGA traces of the pure PES and nanocomposite samples in a nitrogen environment are shown in Fig. 9. The data available

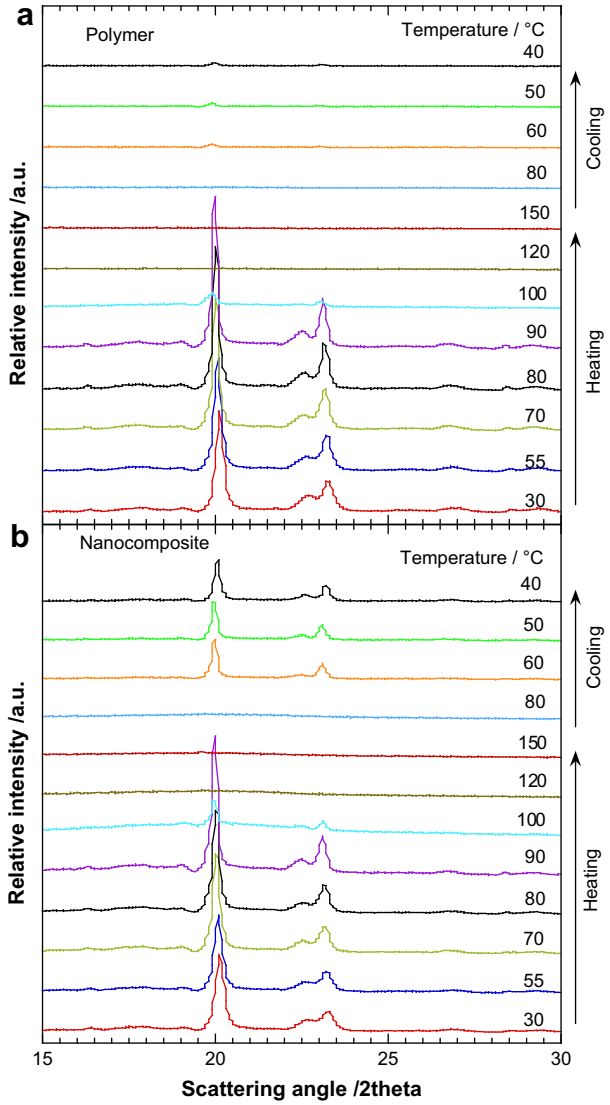

Fig. 8. Temperature dependence wide-angle X-ray scattering patterns of (a) pure polymer and (b) nanocomposite samples during both heating and cooling cycles in SAXSess instrument. Like DSC scans and POM observations, one-dimensional X-ray patterns also show that it is very difficult for pure polymer crystals to grow after melting. For clarity, data were vertically offset.

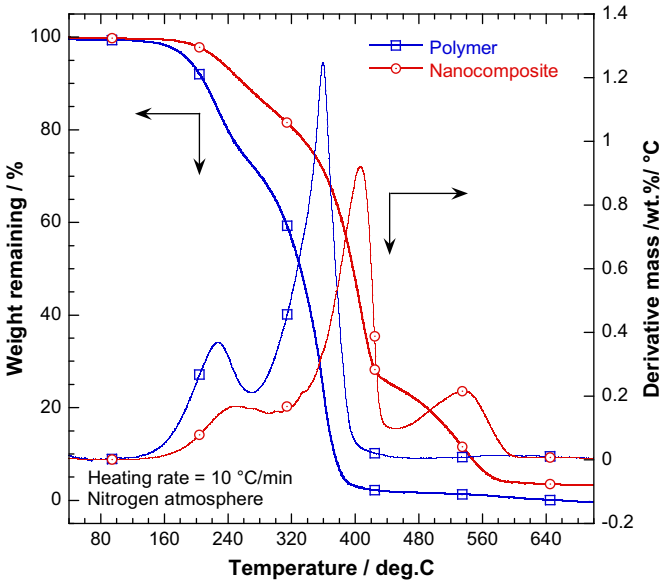

Fig. 9. Thermogravimetric analyses of pure polymer and nanocomposite sample under nitrogen at a heating rate of 10 °C/min. Results show a significant improvement of thermal stability of pure polymer after nanocomposite formation with 5 wt% C30B.

from the TGA scan include: $T_{0.05}$, the temperature at which 5% degradation occurs, which is calculated from the intersection of the tangent of the initial point and considered as the onset temperature of degradation; $T_{0.5}$, the temperature at which 50% degradation occurs, which is another measure of thermal stability; and finally, the non-volatile fraction at 650 °C, denoted as char formation. These data are summarized in Table 3.

It is clear from Fig. 9 and Table 3 that the thermal stability of PES improved after nanocomposite formation with the incorporation of 5 wt% C30B. This improvement in thermal stability of nanocomposite, at all temperature ranges, is due to the homogeneous dispersion of the highly delaminated silicate layers in the PES matrix, which by nature has higher thermal stability [37]. Another reason may be due to the increase in crystallinity of the PES phase in nanocomposite sample as time goes by because the thermal stability of the crystalline phase is much higher than the amorphous one.

The first derivative TGA (dTGA) curves of both samples are also shown in Fig. 9. The dTGA curves are chosen for the presentation, because they more clearly show the difference in thermal stability of all samples studied here. Pure PES sample shows a two-step decomposition process: the first degradation step is mainly due to the chain scission and the second step is related to the complete degradation of polymer chains. On the other hand, the nanocomposite sample shows an extra peak at 520 °C, and we believe this peak is due to the char formation. In the case of the nanocomposite sample, the first two dTGA peaks move to the higher temperature range and the intensities of those peaks decrease significantly in comparison to the pure polymer sample. This indicates that the thermal stability of PES improves significantly after the formation of nanocomposite with C30B. This property improvement is very important for PES nanocomposite based final products.

Table 3
Data summarized from TGA scans. Reported data are averages of three consecutive runs with an uncertainty of ± 1.67 °C.

Sample	$T_{0.05}$/°C	$T_{0.5}$/°C	Char at 650 °C/%
Pure PES	192.5	331.6	0
Nanocomposite	231.5	395.8	3.6

$T_{0.05}$, the temperature at which 5% degradation occurs, which is calculated from the intersection of the tangent of the initial point and considered as the onset temperature of degradation. $T_{0.5}$, the temperature at which 50% degradation occurs.

4. Conclusions

In summary, the effect of incorporation of C30B on the non-isothermal crystallization and melting behaviors and thermal stability of PES was investigated. Structural and morphological analyses reveal the formation of disorder intercalated nanocomposite where intercalated and or exfoliated silicate layers are homogeneously dispersed in the polymer matrix. This is due to the favorable interaction between the poly(ethylene succinate) matrix and the surfactant used to modify the pristine clay. The highly dispersed silicate particles accelerate the mechanism of nucleation and crystal growth of PES by offering huge surface area and also stopping the super-cooling phenomenon of the PES matrix during non-isothermal crystallization. The dramatic improvement in thermal stability of the PES matrix after nanocomposite formation is due to the homogeneous dispersion of the silicate layers in the PES matrix. Another reason may be the higher crystallinity of polymer matrix in the nanocomposite. These improved properties are very important to obtain fully crystallized poly(ethylene succinate) nanocomposite based products or parts in an injection molding cycle.

Acknowledgements

This work was financed by the Council for Scientific and Industrial Research and the Department of Science and Technology, South Africa.

References

[1] Yu L, Dean K, Lin Li. Polymer blends and composites from renewable resources. Prog Polym Sci 2006;31:576–602.
[2] Vink ETH, Rabago KR, Glassner DA, Gruber PR. Applications of life cycle assessment to natureworks polylactide (PLA) production. Polym Degrad Stab 2003;80:403–19.
[3] Ha CS, Cho WJ. Miscibility, properties, and biodegradability of microbial polyester containing blends. Prog Polym Sci 2002;27:759–809.
[4] Sinha Ray S, Bousmina M. Biodegradable polymer and their layered silicate nanocomposites: in greening the 21st century materials science. Prog Mater Sci 2005;50:962–1079.
[5] Fujimaki T. Processability and properties of aliphatic polyesters, "BIONOLLE", synthesized by polycondensation reaction. Polym Degrad Stab 1998;59:209–24.
[6] Tansengco ML, Tokiwa Y. Thermophilic microbial degradation of poly(ethylene succinate). World J Microbiol Boitechnol 1998;14:133–6.
[7] Tezuka Y, Ishii N, Kasuya K, Mitomo H. Degradation of poly(ethylene succinate) by mesophilic bacteria. Polym Degrad Stab 2004;84:115–21.
[8] Ishii N, Inoue Y, Shimada KI, Tezuka Y, Mitomo H, Kasuya KI. Fungal degradation of poly(ethylene succinate). Polym Degrad Stab 2007;92:44–52.
[9] Mergaert J, Webb A, Anderson C, Wouters A, Swings J. Microbial degradation of poly(3-hydroxybutyrate) and poly(3-hydroxybutyrate-co-3-hydroxyvalerate) in soil. Appl Environ Microbiol 1993;59(3):233–8.
[10] Kasuya K, Takagi K, Ishiwatari S, Yoshida Y, Doi Y. Biodegradability of various aliphatic polyesters in natural waters. Polym Degrad Stab 1998;59:327–32.
[11] Tokiwa Y, Suzuki T. Purification and some preperties of polyethylene adipate-degrading enzyme produced by penicillium sp. Strain 14-3'. Agric Biol Chem 1977;41:265–74.
[12] Li S, McCarthy S. Influence of crystallinity and stereochemistry on the enzymatic degradation of poly(lactides)s. Macromolecules 1999;32:4454–6.
[13] Gan Z, Abe H, Doi Y. Biodegradable poly(ethylene succinate) (PES). 1. Crystal growth kinetics and morphology. Biomacromolecules 2000;1:704–12.
[14] Al-Raheli IA, Qudah Ali MA. On the triple melting behaviour of poly(ethylene succinate). Polym Interna 1995;37:249–64.
[15] Ichikawa Y, Kondo H, Igarashi Y, Noguchi K, Okuyama K, Washiyama J. Crystal structure of α and β forms of poly(tetramethylene succinate). Polymer 2000;41:4719–27.
[16] Al-Salah HA. Crystallization and morphology of poly(ethylene succinate) and poly(β-hydroxybutyrate). Polym Bull 1998;41:593–600.
[17] Chen HL, Wang SF. Crystallization induced microstructure of polymer blends consisting of two crystalline constituents. Polymer 2000;41:5157–64.
[18] Qiu ZB, Ikehara T, Nishi T. Unique morphology of poly(ethylene succinate)/poly(ethylene oxide) blends. Macromolecules 2002;35:8251–4.

[19] Sinha Ray S, Okamoto M. Polymer/layered silicate nanocomposites: a review from preparation to processing. Prog Polym Sci 2003;28:1539–641.
[20] Sinha Ray S, Bousmina M. Polymer nanocomposites and their application. Nalwa HS, editor. USA: American publishers; 2006 [chapter 23].
[21] Krevelen DWV. Properties of polymers. Amsterdam, the Netherlands: Elsevier; 1990.
[22] Sinha Ray S, Maiti P, Okamoto M, Yamada K, Ueda K. New polylactide/layered silicate nanocomposites. 1. Preparation, characterization and properties. Macromolecules 2002;35:3104–10.
[23] Sinha Ray S, Yamada K, Okamoto M, Ogami A, Ueda K. New polylactide/layered silicate nanocomposites. 3. High performance biodegradable materials. Chem Mater 2003;15:1456–65.
[24] Sinha Ray S, Yamada K, Okamoto M, Ogami A, Ueda K. New polylactide/layered silicate nanocomposites. 2. Nanoscale control over multiple properties. Macromol Rapid Commun 2002;23:943–7.
[25] Papageorgiou GZ, Bikiaris DN. Crystallization and melting behaviour of three biodegradable poly(alkylene succinates). A comparative study. Polymer 2005;46:12081–92.
[26] Qiu G, Tang Z, Huang N, Gerking L. Dual melting endotherms in the thermal analysis of poly(ethylene terephthalate). J Appl Polym Sci 1998;69:729–42.
[27] Kim HG, Robertson RE. Multiple melting endotherms in isothermally melt-crystallized poly(butylene terephthalate. J Polym Sci Part B Polym Phys 1998;36:1757–67.
[28] Passingham C, Hendra PJ, Cudby MEA, Zichy Z, Weller M. The re-evaluation of multiple peaks in the DSC melting endotherm of isotactic polypropylene. Eur Polym J 1990;26:631–8.
[29] Yasuniwa M, Tsubakihara S, Satou T, Iura K. Multiple melting behavior of poly(butylene succinate). II. Thermal analysis of isothermal crystallization and melting process. J Polym Sci Part B Polym Phys 2005;43:2039–47.
[30] Wang Y, Bhattacharya M, Mano JF. Thermal analysis of the multiple melting behavior of poly(butylene succinate-co-adipate). J Polym Sci Part B Polym Phys 2005;43:3077–82.
[31] Sinha Ray S, Bandyopadhyay J, Bousmina M. Thermal and thermomechanical properties of poly[(butylenes succinate)-co-adipate] nanocomposite. Polym Degrd Stab 2007;92:802–12.
[32] Kong Y, Hay JN. Multiple melting behaviour of poly(ethylene terephthalate). Polymer 2003;44:623–33.
[33] Medellin-Rodriguez FJ, Phillips PJ, Lin JS, Campos R. The triple melting behavior of poly(ethylene terephthalate): molecular weight effects. J Polym Sci Part B Polym Phys 1997;35:1757–74.
[34] Sinha Ray S, Bousmina M. Crystallization behaviour of poly[(butylenes succinate)-co-adipate nanocomposite]. Macromol Chem Phys 2006;207: 1207–19.
[35] Sinha Ray S, Bandyopadhyay J, Bousmina M. Influence of degree of intercalation on the crystal growth kinetics of poly[(butylene succinate)-co-adipate] nanocomposites. Euro Polym J 2008;44:3133–45.
[36] Bandyopadhyay J, Sinha Ray S, Bousmina M. Nonisothermal crystallization kinetics of poly(ethylene terephthalate) nanocomposites. J Nanosci Nanotechnol 2008;8:1812–22.
[37] Sinha Ray S, Bandyopadhyay J, Bousmina M. Effect of organoclay on the morphology and properties of poly(propylene)/poly[(butylene succinate)-co-adipate] blends. Macromol Mater Eng 2007;292:729–47.